Journal of Materials Chemistry B

Accepted Manuscript

ROYAL SOCIETY OF CHEMISTRY

www.rsc.org/materialsB

Journal of Materials Chemistry B RSCPublishing

ARTICLE

Magnetic biopolymer nanogels via biological assembly for vectoring delivery of biopharmaceuticals

Cite this: DOI: 10.1039/xoxxoooooox

Received ooth January 2012,
Accepted ooth January 2012

DOI: 10.1039/xoxxoooooox

www.rsc.org/

Ming Fan[a], Jingxuan Yan[a], Huaping Tan*[a], Yuting Miao[a] and Xiaohong Hu[b]

Biopolymer-based nanogels have great potential in the field of tissue regenerative medicine. In this work, a magnetic biopolymer nanogel via specific nucleobase pairing was developed for vectoring delivery of cell growth factor. The biopolymer nanogel basing chitosan and heparin was established by the Watson-Crick base pairing between thymine and adenine via the hydrogen bonding. The magnetic biopolymer nanogels exhibit quick magnetic responsibility, which was fabricated by encapsulating super-paramagnetic iron oxide nanoparticles. The potential application of this magnetic nanogel on vectoring delivery of cell growth factor was confirmed by adsorption and release behaviors of bone morphogenetic protein 2 (BMP-2). The existence of heparin made the nanogel achieve high loading efficiency of BMP-2, and the vectoring delivery of BMP-2 could be easily controlled by the external magnetic field. *In vitro* cytotoxicity tests demonstrated that incorporation of BMP-2 into this biopolymer nanogel through binding with heparin showed high efficiency to promote MG-63 cells viabilities, in particular under magnetic field, which suggested a promising future for cartilage and bone regeneration applications.

1. Introduction

In tissue engineering, biodegradable hydrogels have served as highly functional scaffolds for cells and growth factors (GFs) which increases the effectiveness in regulation of cell proliferation and differentiation.[1] The recent convergence of biomaterials and nanotechnology has enabled the development of intelligent hydrogel-based cell scaffolds, e.g., nanogels, with the particle size smaller than 200 nm.2 Nanogels involve the incorporation of nanoparticles with a hydrophilic matrix, which can improve the properties of conventional bulk hydrogel systems. In tissue engineering and regenerative medicine, nanogels provide unique properties to address challenges such as modifiable mechanical and interfacial properties of a cell scaffold to mimic native extracellular matrix (ECM).

Cell scaffolds should be able to provide stabilization of GFs activity and prolonged delivery during tissue regeneration. A major issue in the use of nanogel scaffold is that the establishment of a vectoring delivery is necessary for ensuring the GFs targets the defect site. Recently, super-paramagnetic iron oxide nanoparticles have been widely used in biomedical applications, such as cell patterning, blood purification, targeted drug delivery, clinical imaging, and biosensors for *in vivo* biomarker detection.[3] Especially, these magnetic materials have particularly high potential for vectoring agents in the treatment of tumors by hyperthermia techniques. Furthermore, due to their innate magnetic characteristics and biocompatibility, magnetic nanoparticles have been encapsulated in biomaterials to fabricate novel cell scaffolds. For example, iron oxide nanoparticles have been integrated with hydrogels via microfluidics, to form multiplexed bioassays and to generate scaffolds for on-demand drug and cell delivery.[4]

Many crosslinking agents have been employed for the preparation of cell scaffolds, including carbodiimide, glutaraldehyde and genipin. However, these chemical crosslinking agents are the major obstacles in the use as nanogels due to their toxicity to cells and GFs, thus limiting their applications on tissue engineering.[5] Recently, biological assembly has the ability to overcome these obstacles through local delivery of chemotherapeutic agents in therapeutic doses, increasing treatment efficacy and decreasing adverse effects.[6] In the past few years, the use of specific nucleobase pairing as a driver for self-assembly has been known in supramolecular chemistry. Assembly of biopolymers through specific nucleobase pairing has been employed for preparation of membranes and hydrogels for biomedical applications.[7] These successful results clearly illustrate that specific nucleobase pairing promise as scaffolding materials for cell cultures and tissue engineering.

We hypothesize that nanogel approach using magnetic nanoparticles, the magnetic nanogel, has potential to broad tissue engineering and pharmaceutical applications, such as vectoring delivery of GFs to target the defect sites of cartilage and bone. The magnetic nanogel can be fabricated as microscale building blocks and manipulated under controlled magnetic fields to create tissue constructs using bottom-up tissue engineering approaches. Herein,

we describe a novel combined approach of emulsification-precipitation polymerization to prepare magnetic biopolymer nanogels via nucleobase pairing. Biopolymers such as chitosan and heparin have been extensively applied in the hydrogels due to its versatility, biocompatibility, functionality, safety, and biodegradability. This study describes the synthesis, characterization, *in vitro* drug release and cytotoxicity of a chitosan/heparin composite nanogel with super-paramagnetic characteristics, as a GF delivery system for cartilage and bone tissue engineering.

2. Experimental Section

Materials

Adenine, thymine, heparin (sodium salt, Mw 18 kDa), chitosan (deacetylation degree 85%, Mw 130 kDa) and 3-(4,5-dimethyl-thiazol-2-yl)-2,5-diphenyltetrazolium bromide (MTT) were purchased from Sigma-Aldrich. Recombinant human BMP-2 (rhBMP-2) and the BMP-2 Quantikine ELISA Kit were obtained from R&D Systems (Minneapolis, USA). All other chemicals were used as received without purification.

Synthesis of nucleotide modified biopolymers

Diethyl ether (0.07 mmol) and $CHCl_3$ (0.035 mmol) was added to phosphorus pentoxide (0.035 mmol) with stirring and the mixture was heated under reflux for 12 h at 50 °C to get a clear solution. The solvent is then distilled off under vacuum to obtain polyphosphate ester. Adenine (0.004 mmol) was dissolved in 50 mL of dimethylformamide with the addition of 0.25 mL of concentrated HCl with magnetic stirring. Polyphosphate ester was added to chitosan (0.0006 mmol) in 30 mL of dimethylformamide, followed by dropwise addition of adenine solution, and the mixture was heated to 50 °C for 24 h. The reaction was cooled at RT and dimethylformamide is distilled off *in vacuo*. The moist residue is dissolved in water and kept in an ice-box for about 1 h to precipitate unreacted adenine. To the clean aqueous layer, ammonia is added to bring the pH to 10. The ammonia layer was extracted with ethyl acetate and the organic layer is evaporated. The product was dissolved in water and further purified by dialysis (MWCO 10,000) against ultrapure water for 3 days. The purified solution was lyophilized to give a solid foam.

The clear solution of thymine (0.004 mmol) was obtained by dissolving in 25 mL of H_2O with the addition of 0.25 mL of concentrated HCl solution. Polyphosphate ester was added to heparin (0.0008 mmol) in 50 mL of H_2O, followed by dropwise addition of thymine, and the mixture was heated to 50 °C for 20 h and cooled under ice for about 1 h to precipitate unreacted thymine. The acid layer is neutralized by the addition of ammonia. The ammonia layer was extracted with ethyl acetate and the organic layer is evaporated. The product was dissolved in water and further purified by dialysis (MWCO 3,500) against ultrapure water for 3 days. The purified solution was lyophilized to give a solid foam.

For brevity, the adenine functionalized chitosan and thymine functionalized heparin are designated as chitosan-Ade and heparin-Thy, respectively. The nucleotide functionalities of the chitosan-Ade and heparin-Thy were characterized via ^{1}H NMR (Bruker Avance). ^{1}H NMR spectroscopy results indicated that the nucleotide functionalities on chitosan and heparin were estimated to be 47.3% and 62.3%, respectively.

Assembly of nanogels

The preparation of Fe_3O_4 nanoparticles was followed by a chemical co-precipitation of Fe^{2+} and Fe^{3+} ions described previously.[4] With some modifications, 28 mmol $FeCl_2$ and 16 mmol $FeCl_3$ were prepared in 50 mL deionized water in two beakers, and then transferred to a 250 mL three-necked flask together, stirred under nitrogen. When the solution was heated to 60°C, $NH_3 \cdot H_2O$ (25 wt%) was added drop wise until pH 10. After base was added, the solution immediately became dark brown, which indicates iron oxide has been formed in the system. The solution was heated at 80°C for 1 h. The precipitates were isolated from the solvent by magnetic decantation and repeatedly washed with deionized water until neutral, then were dried at room temperature under vacuum for 24 h.

Biopolymer-based nanogels were prepared by assembly of chitosan-Ade and heparin-Thy in an inverse emulsion via the inverse emulsion cross-linking technique. Chitosan-Ade and heparin-Thy were dissolved in ultrapure water to form precursor solutions at concentrations of 0.5~2.0 wt%. For the assembly of nanospheres, solutions of chitosan-Ade (0.5 wt%) and heparin-Thy (2.0 wt%) were respectively added equal weight of Fe_3O_4 nanoparticles and thoroughly mixed with 1:1 volume ratio at room temperature by vigorous pipetting. The inverse emulsion was prepared by homogenizing nucleotide functionalized biopolymers (4 mL) in mineral oil (80 mL) containing 0.5 mL of Span 80 for 5 min using a homogenizer. The aqueous phase was allowed to evaporate overnight at 37 °C with constant stirring. Magnetic nanoparticles were isolated by precipitation in a large excess of isopropyl alcohol followed by centrifugation to remove the oil phase. The resulting nanoparticles were filtered and thoroughly washed with distilled water, isopropyl alcohol, hexane, and acetone before being dried under vacuum for 24 h at room temperature.

Fourier transformed infrared (FT-IR) spectra of the obtained nanoparticles were measured to confirm the chemical composition. The obtained sample was recorded with FT-IR spectrometer (Nicolet Avatar 360, USA) against a blank KBr pellet background. Thermal gravimetric analysis (TGA) of the obtained nanoparticles was performed on a thermo-gravimetric analyzer (Pyris 1, Perkin Elmer) by heating from room temperature to 650 ^{o}C at a rate of 20 ^{o}C/min with a nitrogen flow rate of 20 mL/min.

The nanogel was obtained by immersing nanoparticles in phosphate buffered saline (PBS) in presence of BMP-2 at 37 ^{o}C for 1 h to allow equilibrium of swelling. For preparation of GFs-loaded nanogels, BMP-2 was dissolved in PBS to form series solutions with different concentrations (1, 3, 5, 7, 10 μg/mL). The nanogels were collected by magnetic decantation to remove excess buffer. The average diameters of the nanogels were determined using a Malvern Zetasizer Nano ZS instrument at room temperature.

Characterization of nanogels

Morphology

Morphologies of the magnetic nanogel were characterized by utilizing scanning electron microscopy (SEM) and transmission electron microscopy (TEM). The swollen magnetic nanogel was critical point dried (Emitech-K850, Quorum, UK) and then gold-coated. The morphology was viewed using a Hitachi-SU8010 SEM (Hitachi, Japan) operated at 12 kV accelerating. TEM micrograph of samples was taken by a JEM-1011 TEM (JEOL, Peabody, MA) operated at 200 kV.

Magnetic measurement

The magnetic hysteresis (M-H) curves of the magnetic nanogels were measured at 300 K with a magnetic field between -20 and 20 kOe using a superconducting quantum interference device magnetometer (Lake Shore 7400, USA).

Degradation and swelling

Weight loss of initially weighed nanogels (W_0) was monitored as a function of incubation time in PBS at 37°C in the presence of 1 mg/mL lysozyme. At specified time intervals, nanogels were removed from the PBS and weighed (W_t). The weight loss ratio was defined as $100\%\times(W_0-W_t)/W_0$. The weight remaining ratio was defined as $1-100\%\times(W_0-W_t)/W_0$. For swelling experiment, the nanogels were immersed in PBS, and kept at 37°C for 2h until equilibrium of swelling had been reached. At predetermined intervals, the nanogels were centrifuged and immediately weighed (Ws). The nanogels were then lyophilized at -50 °C and weighted (Wd). The swelling ratio was calculated using the equation of SR = (Ws–Wd)/Wd.

GFs release

For *in vitro* release experiment, BMP-2-loaded nanogels (10 mg) were suspended in 1 mL of PBS at 37 °C, provided a reservoir into which peptide could be released from the scaffolds complex and subsequently measured during degradation. At predetermined intervals, a 200 μL sample of release medium was extracted from the sample vials and replenished with 200 μL fresh release medium to maintain a constant volume. Samples were centrifuged and supernatants were collected and stored at -80 °C until analysis by the immunoassay measurement.

Cytotoxicity tests

Human osteoblasts MG-63 were seeded at a density of 1×10^4 cells per well in a 96-well culture plate and incubated for 12 h in the incubator. Cells were treated with culture medium containing non-magnetic nanogels or magnetic nanogels at different concentrations (20~160 μg/mL) and incubated for another 24 h. Cells were then washed with PBS 3 times to remove free nanogels. Cytotoxicity of nanogels was further determined by MTT assay. MTT solution (0.5 mg/mL in PBS, 75 μL) was added to each well and incubated for 4 h. After the supernatant was removed, dimethyl sulfoxide (150 μL) was added to dissolve the formazan crystals. The absorbance of each well was measured at 550 nm by a multi-mode plate reader (SpectraMax M5, Molecular Devices, USA) in the UV-visible mode.

Statistical analysis

The experimental data from all the studies were analyzed using Analysis of Variance (ANOVA). Statistical significance was set to p value ≤ 0.05. Results are presented as mean ± standard deviation.

3. Results and discussion

Nanogel Synthesis

Nanogels should be able to provide stabilization of GFs activity and vectoring delivery during tissue regeneration. We present a flexible way to assemble a magnetic nanogel via specific pairing of functionalized nucleobases that are capable of vectoring delivery. The magnetic biopolymer hydrogel system is established by the Watson-Crick base pairing between thymine and adenine via the hydrogen bonding. Our strategy is to use biopolymer derivatives, e.g. chitosan and heparin, as the nanogel precursors. Chitosan is composed of repeated glucosamine and *N*-acetylglucosamine, which has been applied in tissue engineering, drug delivery and gene therapy due to its biodegradability, biocompatibility and antibacterial properties.[8] Heparin is composed of repeated disaccharide units of alternating glucosamine and glucuronic residues heterogeneously modified by carboxyl groups and *N*- or *O*-linked sulfate. The ability of heparin to sequester and stabilize GFs due to specific affinity interaction has been exploited in the production of scaffolds that can mediate cell proliferation and differentiation.[9]

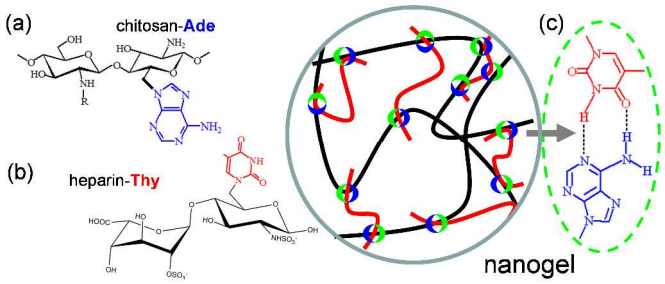

Fig. 1. Schematic assembly of nanogel through the Watson-Crick nucleobase pairing between chitosan and heparin. The nanogel precursors were designed with adenine and thymine on chitosan and heparin backbone respectively, which are accessible for nucleobase pairing via the hydrogen bonding.

For nucleobase pairing, chitosan and heparin were functionalized with adenine and thymine functionalities as assembly precursors (referred as chitosan-Ade and heparin-Thy), respectively (**Fig. 1a** and **1b**). After dissolution and mixture of precursors in an aqueous environment, a nucleobase paired chitosan/heparin composite was assembled due to the formation of pairing complexes via hydrogen bonding (**Fig. 1c**). Magnetic nanogels were formed by encapsulating super-paramagnetic Fe_3O_4 nanoparticles. To investigate the utility and versatility of the nanogel for GFs release, the bone morphogenetic protein (BMP-2) was employed as the model for vectoring delivery.

Nanogel Structures

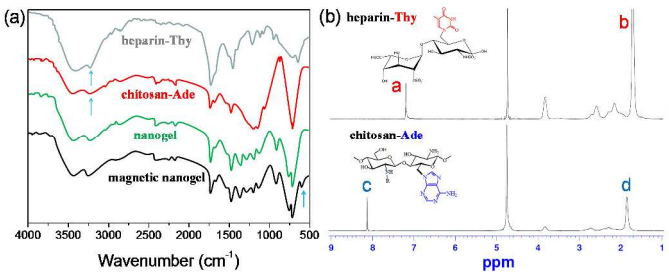

Fig. 2. (a) FT-IR spectra of thymine functionalized heparin (heparin-Thy), adenine functionalized chitosan (chitosan-Ade), non-magnetic nanogel and magnetic nanogel. (b) ^{1}H NMR spectra of heparin-Thy and chitosan-Ade.

The formation of heparin-Thy and chitosan-Ade was confirmed by FT-IR and ^{1}H NMR measurement. The FT-IR spectra of the biopolymers and magnetic nanogel are shown in **Fig. 2a**. The decrease of the band at 3245 cm^{-1} in the heparin-Thy indicates that it undergoes a condensation reaction with the primary -OH group of heparin, and the appearance of a new band at 1342 cm^{-1} is due to the

C-N stretching vibration between heparin and thymine. In the spectrum of chitosan-Ade, a characteristic band at 3254 cm^{-1} and a transmittance peak at 2975 cm^{-1} can be assigned to the -NH stretching of adenine and chitosan, respectively. The appearance of a new peak at 1115 cm^{-1} in chitosan-Ade, which corresponds to the C-N stretching vibration, indicating the functionalization of chitosan by adenine. The FT-IR spectrum of magnetic nanogel was obtained similar to magnetic-free nanogel with additional absorption peaks at 580 cm^{-1} that could be assigned to Fe-O bonds of Fe_3O_4 nanoparticles.[4] The functionalization was also confirmed by ^1H NMR (**Fig. 2b**). As shown in spectrum of heparin-Thy, the peak at 7.21 ppm is due to the -CH protons of thymine, and the peak at 1.68 ppm corresponds to the $-CH_3$ protons of thymine. In spectrum of chitosan-Ade, the peaks at 8.12 and 1.85 ppm are assigned to -CH and $-NH_2$ protons of adenine, respectively.

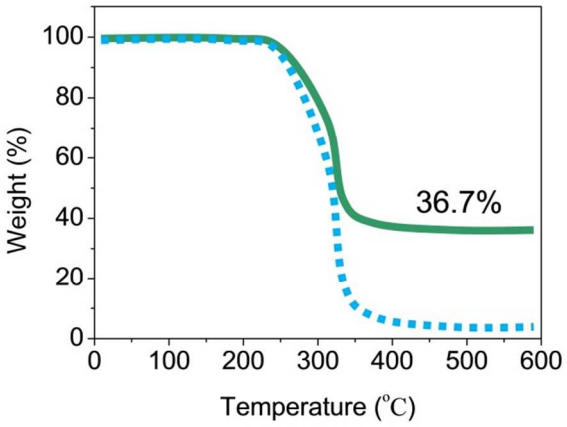

Fig. 3. TGA curves of the as-obtained non-magnetic nanogels and magnetic nanogels.

TGA was performed to measure the component of the magnetic nanogels. **Fig. 3** shows the TGA curve of the nanoparticles with magnetic Fe_3O_4, and the other nanoparticles without magnetic iron oxide was also investigated as control group. Comparing to the control nanoparticles, the weight percentage of the burning residues was 36.7% for the magnetic nanoparticles. It is obvious that the actual proportion of magnetic iron oxide in the as-obtained nanoparticles was in good accordance with the feed ratio in the reaction mixtures, which reflects that the monomer conversion was relatively high for the *in situ* encapsulations in the presence of magnetic iron oxide.

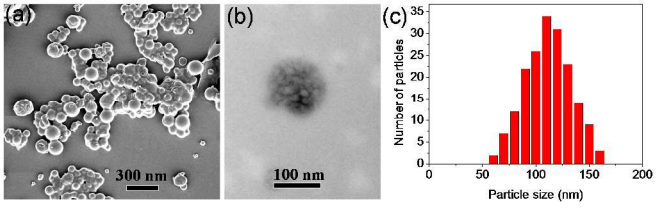

Fig. 4. (a) SEM image of magnetic nanogels. (b) TEM image of magnetic nanogels. (c) Histogram of the particle size distribution.

SEM was conducted to examine the morphology and architecture of the magnetic nanogels. SEM image in **Fig. 4a** shows that the products are composed of well dispersed nanoparticles with spherical morphologies. The TEM image in **Fig. 4b** further confirms encapsulation of the Fe_3O_4 nanoparticles within the nanogels. The number-averaged size of magnetic nanogels determined by dynamic light scattering (DLS), which showed the particle size distribution fitted with lognormal distribution (**Fig. 4c**). Size of these nanoparticles ranges from ~60 nm to ~160 nm, and the calculated average particle diameter was 109.4 nm, which was consistent with SEM observation in **Fig. 4a**.

Nanogel Properties

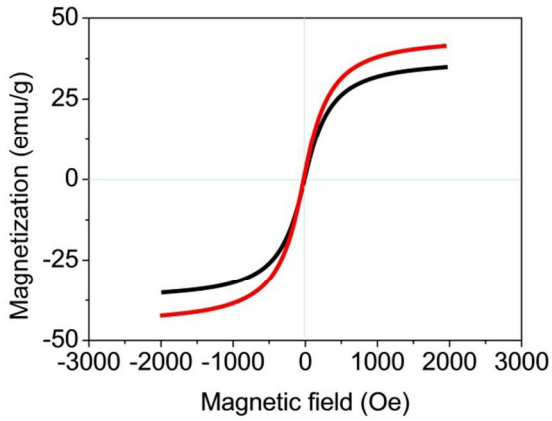

Fig. 5. The magnetic hysteresis curves of Fe_3O_4 nanoparticles and magnetic nanogels.

Magnetic hydrogels have been investigated and applied in biomedical procedures, because they can be stimulated by magnetic field. The magnetic behavior of prepared Fe_3O_4 nanoparticles and Fe_3O_4 encapsulated nanogel measured at room temperature is shown in **Fig. 5**. The saturation magnetization value of magnetic nanogel was 38.8 emu/g, which was a little lower than that of Fe_3O_4 (48.2 emu/g). This magnetic behavior indicated no hysteretic effect on the magnetic nanogel. These results confirmed that the super-paramagnetic property was mostly retained after encapsulation in this biopolymer nanogel.

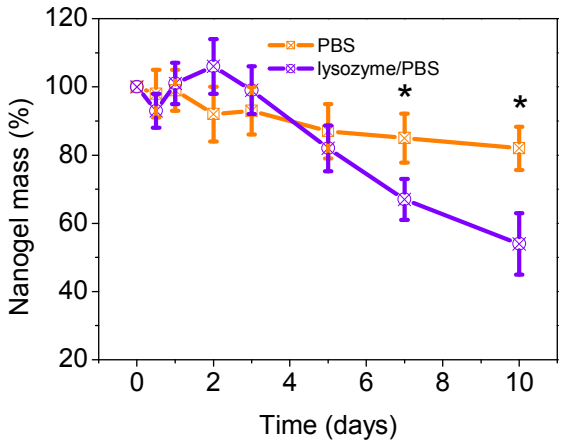

Fig. 6. Degradation of magnetic nanogels in PBS with or without 1 mg/mL lysozyme at 37°C with respect to weight loss. Values reported are an average n = 5, ± standard deviation.

The degradation properties of the magnetic nanogel were monitored as a function of incubation time in PBS at 37°C. As

shown in **Fig. 6**, the magnetic nanogels lost their weight steadily up to 10 days. At day 10, the weight remaining ratio of magnetic nanogel was 81.6%. Since chitosan is an enzymatically degradable polysaccharide, the enzymatic resistance of magnetic nanogel was also investigated in a lysozyme solution (1 mg/mL PBS) as a function of incubation time. The lysozyme resulted in a significant mass loss (p<0.05), and the weight remaining ratio of magnetic nanogel was 54.5% after incubation for 10 days.

Swelling properties of the nanogels are crucial for substance exchange when used for biopharmaceuticals delivery. To examine responses to external stimuli, the swelling kinetics of the magnetic nanogel was investigated in response to enzymatic incubation in PBS (**Fig. 7**). The results showed that the magnetic nanogel underwent significant volume changes with enzymatic incubation. The enzyme also significantly enhanced swelling of the nanogels over culture time (p<0.05). When incubated for 600 min, the swelling ratio of the gel steadily increased to 7.1, not fragmenting at any of these temperatures, which was significantly higher than the one in regular PBS, 4.2.

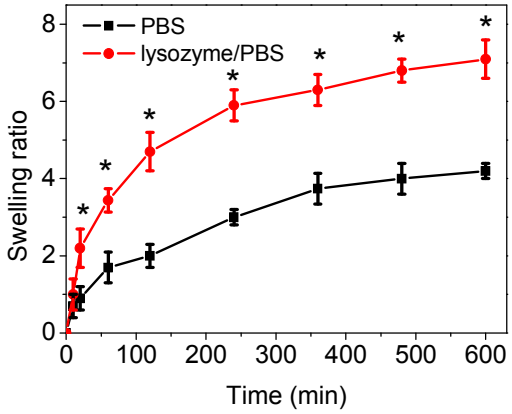

Fig. 7. Swelling kinetics of magnetic nanogels in PBS with or without 1 mg/mL lysozyme as a function of incubation time at 37°C. Values reported are an average n = 5, ± standard deviation.

Vectoring Delivery of BMP-2

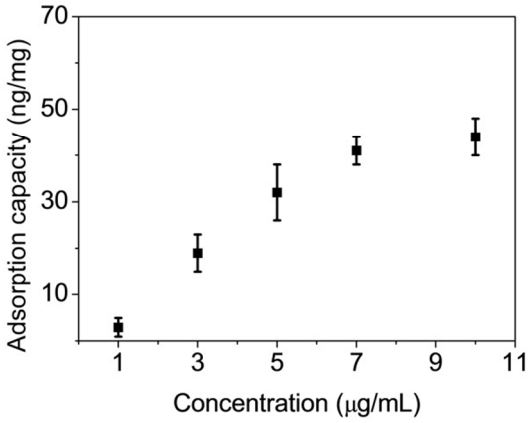

Fig. 8. Adsorption capacity of BMP-2 by magnetic nanogels in PBS as a function of feeding concentration at 37°C. Values reported are an average n = 5, ± standard deviation.

Fig. 8 shows the adsorption capacity of BMP-2 by magnetic nanogel after one hour of contact with a solution of BMP-2 at concentrations of 1 to 10 μg/mL in PBS at 37°C, with the application of the Langmuir-Freundlich mathematical model. The results showed that the adsorption of BMP-2 increased along with feeding concentrations of BMP-2. At various feeding concentrations of BMP-2, the adsorption capacity of BMP-2 increased gradually from 3.1 ng/mg at 1 μg/mL to 41.3 ng/mg at 7 μg/mL. After that, the adsorption percentage increased very slowly. It is expected that the incorporated heparin in the nanogels should correlate with the amount of the adsorbed BMP-2. The magnetic nanogel has a high adsorption capacity of BMP-2 at the concentration of 10 μg/mL and the maximum adsorption capacity was 43.6 ng/mg with the application of the Langmuir-Freundlich isotherm. This high capacity of the magnetic nanogel is required for use in delivery systems. Since the binding of heparin into the nanogel is the bridge between the nanogel and BMP-2, the BMP-2 are easily captured by the heparin via affinity interactions.[9] Our magnetic nanogel based on heparin and chitosan presented high adsorption capacity of BMP-2 than other carriers described in the literature. High adsorption capacities of cell growth factor proteins would result opsonization and prolong the circulation time of the nanogel as cell scaffolds *in vivo*.

Controlled release of GFs can be achieved through their anchorage at predetermined locales of the heparin incorporated nanogel system. To evaluate the ability of effectively deliver GFs, the *in vitro* cumulative amount of BMP-2 released from the magnetic nanogel (41.3 ng/mg BMP-2/nanogel) at specific time points was quantified. As observed in **Fig. 9a**, the magnetic nanogels incubated in PBS at 37°C demonstrated a total cumulative release of approximately 22.3% over the 24 h time period. In comparison to the lower release from the magnetic nanogel, the control nanogel showed a increase in the burst release to a higher level and decrease the sustained release to a long duration, with a value of 36.5%. There is a large difference in the final amount released, but when they are incorporated into the nanogel, the BMP-2 were released more slowly, indicating a sustained release. The GFs might be easily accessible to heparin, thus enabling affinity interactions in aqueous environment.

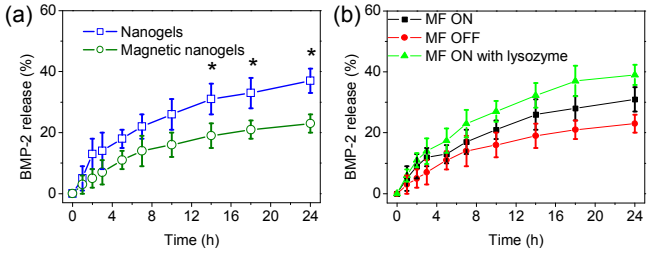

Fig. 9. (a) Cumulative release profiles of BMP-2 from non-magnetic nanogels and magnetic nanogels as a function of time in PBS at 37°C. (b) Cumulative release profiles of BMP-2 from magnetic nanogels as a function of time with or without the application of an external magnetic field in PBS at 37°C. Values reported are an average n = 5, ± standard deviation.

We are interested in utilizing this magnetic nanogel for vectoring delivery of BMP-2 to target the defect sites of cartilage or bone. To demonstrate the utility and versatility of the gel scaffolds for vectoring delivery, the *in vitro* cumulative amount of BMP-2 released from the magnetic nanogel at magnetic field was also quantified. As displayed in **Fig. 9b**, there was a release of 31.2% for

BMP-2 after 24 h incubation when exposured to the magnetic field in PBS at 37°C, which showed slightly higher than the release without magnetic field, but no difference was found between them (p>0.05). Since swelling ratio of the nanogels was increased in the presence of 1 mg/mL lysozyme, the BMP-2 release also showed slightly higher than the release without the enzyme.

At normal physiological pH and temperature, BMP-2 diffuses rapidly when delivered without stabilization, undergoes proteolysis, and consequently loses bioactivity. BMP-2 is known as heparin-binding growth factor because of its high affinity for heparin and heparan sulfate.[9] Binding with heparin can protect from proteolytic degradation and maintain a capacity of long-term biological functions. These results clearly illustrated the potential for BMP-2 loaded nanogels and suggest opportunities for cell encapsulation.

Cytotoxicity of nanogels

For tissue therapy, the toxicity of the magnetic nanogel is a major concern. To evaluate the cell response to the magnetic nanogel loaded with BMP-2 (41.3 ng/mg BMP-2/nanogel), *in vitro* osteoblasts MG-63 culture was performed, using the non-magnetic nanogel as the control. To examine the cytotoxicity of nanogels, MG-63 cells were incubated with different concentrations of the nanogels for 24 h. MTT assay showed that the magnetic nanogels had no restrict effects on the growth of osteoblasts MG-63 at the concentration range of 20~160 μg/mL. Since BMP-2 is a primary promoter of cell proliferation and differentiation of osteoblasts, the cell viabilities of the BMP-2 loaded nanogels were significantly stronger than those of the non-nanogel treated samples (p<0.05), while no significant difference (p>0.05) was found between the magnetic nanogels and the non-magnetic nanogels (p<0.05) (**Fig.10a**). Even at the lowest concentration of nanogels, e.g. 20 μg/mL, the relative cell viability was still over 120%. These data indicated that the magnetic nanogels obtained by our method are bioactive.

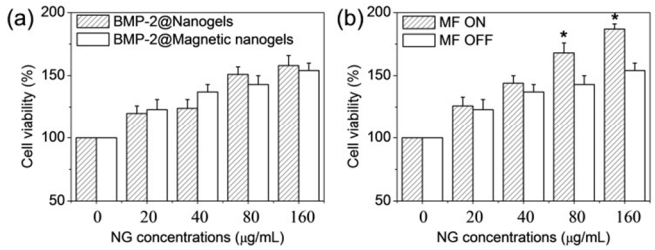

Fig. 10. (a) Cell viability of osteoblasts MG-63 incubated with different concentrations of BMP-2 loaded non-magnetic nanogels and magnetic nanogels for 24 hours. (b) Cell viability of osteoblasts MG-63 incubated with different concentrations of BMP-2 loaded magnetic nanogels with or without the application of an external magnetic field for 24 hours. Values reported are an average n = 5, ± standard deviation.

Furthermore, the cell viabilities with the 80~160 μg/mL magnetic nanogels under magnetic field were significantly stronger than those of the nanogels without magnetic field (p<0.05) (**Fig.10b**). This has demonstrated that incorporation of BMP-2 into this biopolymer nanogel through binding with heparin shows higher efficiency to promote cell viabilities, in particular under magnetic field. Incorporation of magnetic force may improve the interaction of the cell-material interaction; thus the resulting BMP-2 loaded magnetic nanogels showed synchronous effects on the cell behavior by biologically species-specific stimulus.

4. Conclusions

A new strategy has been demonstrated for fabricating magnetic nanogels through specific nucleobase pairing that exhibit quick magnetic responsibility and great biocompatibility. Composition and structure analyses have proven that the magnetic nanogels consist of the Fe_3O_4, chitosan and heparin. In the multifunctional nanogels, the vectoring delivery of BMP-2 could be easily controlled by external magnetic field. The existence of heparin made the nanogel achieve high loading efficiency of BMP-2, and the duration release of BMP-2 from this nanogel was much lower under physiological conditions. *In vitro* cytotoxicity tests demonstrated that the BMP-2 loaded magnetic biopolymer nanogels showed high efficiency to promote MG-63 cells viabilities, in particular under magnetic field. Thus, our multifunctional nanogels basing biopolymers have great potential in future cartilage and bone tissue regeneration applications.

Acknowledgements

This study is financially supported by National Natural Science Foundation of China (51103071, 51103066), the Scientific Research Foundation for Returned Scholars, Ministry of Education of China, Natural Science Foundation of Jiangsu Province (BK2011714) and Zijin Intelligent Program of NJUST.

Notes and references

[a] School of Materials Science and Engineering, Nanjing University of Science and Technology, Nanjing 210094, China. E-mail: hptan@njust.edu.cn.
[b] School of Material Engineering, Jinling Institute of Technology, Nanjing 211169, China.

1. (a) C. A. DeForest, B. D. Polizzotti and K. S. Anseth, *Nat. Mater.,* 2009, **8**, 659. (b) D. A. Wang, S. Varghese, B. Sharma, I. Strehin, S. Fermanian, J. Gorham, D. H. Fairbrother, B. Cascio and J. H. Elisseeff, *Nat. Mater.,* 2007, **6**, 385. (c) G. A. Hudalla, J. T. Koepsel and W. L. Murphy, *Adv. Mater.,* 2011, **23**, 5415. (d) J. D. Kretlow, L. Klouda and A. G. Mikos, *Adv. Drug Deliv. Rev.,* 2007, **59**, 263. (e) M. P. Lutolf, G. P. Raeber, A. H. Zisch, T. Nicola and J. A. Hubbell, *Adv. Mater.,* 2003, **15**, 888.
2. (a) P. D. Thornton, R. J. Mart and R. V. Ulijn, *Adv. Mater.,* 2007, **19**, 1252. (b) H. Wang, O. C. Boerman, K. Sariibrahimoglu, Y. Li, J. A. Jansen and S. C.G. Leeuwenburgh, *Biomaterials,* 2012, **33**, 8695. (c) V. Mironov, R. P. Visconti, V. Kasyanov, G. Forgacs, C. J. Drake and R. R. Markwald, *Biomaterials,* 2009, **30**, 2164. (d) H. Tan, J. Wu, D. Huang and C. Gao, *Macromol. Biosci.,* 2010, **10**, 156. (e) H. Tan, M. Fan, Y. Ma, J. Qiu, X. Li and J. Yan, *Adv, Healthc, Mater.,* 2014, doi: 10.1002/adhm.201400123.
3. (a) A. M. Pavlov, B. G. De Geest, B. Louage, L. Lybaert, S. De Koker, Z. Koudelka, A. Sapelkin and G. B. Sukhorukov, *Adv. Mater.,* 2013, **25**, 6945. (b) F. Xu, F. Inci, O. Mullick, U. A. Gurkan, Y. Sung, D. Kavaz, B. Li, E. B. Denkbas and U. Demirci, *ACS Nano,* 2012, **6**, 6640. (c) X. Zhao, J. Kim, C. A. Cezar, N. Huebsch, K. Lee, K. Bouhadir and D. J. Mooney, *Proc. Natl. Acad. Sci.,* 2011, **108**, 67. (d) H. Tan, X. Gao, J. Sun, C. Xiao and X. Hu, *Chem. Commun.,* 2013, **49**, 11554.
4. (a) M. D. Krebs, R. M. Erb, B. B. Yellen, B. Samanta, A. Bajaj, V. M. Rotello and E. Alsberg, *Nano Lett.,* 2009, **9**, 1812. (b) C. C. Berry, S. Wells, S. Charles and A. S. Curtis, *Biomaterials*, 2003, **24**, 4551. (c) F. Xu, S. J. Moon, A. E. Emre, E. S. Turali, Y. S. Song, S. A. Hacking, J. Nagatomi and U. Demirci, *Biofabrication*, 2010, **2**, 014105. (d) A. K. Gupta and A. S. Curtis, *J. Mater. Sci.: Mater. Med.,* 2004, **15**, 493.
5. (a) H. Tan, C. M. Ramirez, N. Miljkovic, H. Li, J. P. Rubin and K. G. Marra, *Biomaterials,* 2009, **30**, 6844. (b) H. Tan, Q. Shen, X. Jia, Z. Yuan and D. Xiong, *Macromol. Rapid Commun.,* 2012, **33**, 2015. (c) H. Tan, J. P. Rubin and K. G. Marra, *Macromol. Rapid Commun.,* 2011,

32, 905. (d) H. Tan, H. Li, J. P. Rubin and K. G. Marra, *J. Tissue Eng. Regen. Med.,* 2011, **5**, 790.

6. (a) D. G. Anderson, J. A. Burdick and R. Langer, *Science,* 2004, **305**, 1923. (b) J. Zhang, H. Sun and P. X. Ma, *ACS Nano,* 2010, **4**, 1049. (c) T. Vermonden, R. Censi and W. E. Hennink, *Chem. Rev.,* 2012, **112**, 2853. (d) Q. Wang, Z. Yang, X. Zhang, X. Xiao, C. K. Chang and B. Xu, *Angew. Chem. Int. Ed.,* 2007, **46**, 4285.
7. (a) U. Manna, S. Bharani and S. Patil, *Biomacromolecules,* 2009, **10**, 2632. (b) H. Tan, C. Xiao, J. Sun, D. Xiong and X. Hu, *Chem. Commun.,* 2012, **48**, 10289.
8. (a) H. Tan, C. R. Chu, K. A. Payne and K. G. Marra, *Biomaterials,* 2009, **30**, 2499. (b) H. Tan, L. Lao, J. Wu, Y. Gong and C. Gao, *Polym. Adv. Technol.,* 2008, **19**, 15. (c) H. Tan, J. Wu, L. Lao and C. Gao, *Acta Biomater.,* 2009, **5**, 328.

(a) M. J. B. Wissink, R. Beernink, J. S. Pieper, A. A. Poot, G. H. M. Engbers, T. Beugeling, W. G. van Aken and J. Feijen, *Biomaterials,* 2001, **22**, 2291. (b) X. Xu, A. K. Jha, R. L. Duncan and X. Jia, *Acta Biomater.,* 2011, **7**, 3050. (c) N. Chinen, M. Tanihara, M. Nakagawa, K. Shinozaki, E. Yamamoto, Y. Mizushima and Y. Suzuki, *J. Biomed. Mater. Res.,* 2003, **67A**, 61. (d) H. Tan, Q. Zhou, H. Qi, D. Zhu, X. Ma and D. Xiong, *Macromol. Biosci.,* 2012, **12**, 621.